USE OF MICRO X-RAY ABSORPTION SPECTROSCOPY AND DIFFRACTION TO DELINEATE Cr(VI) SPECIATION IN COPR

M. CHRYSOCHOOU[1,*]
D.H. MOON[2]
S. FAKRA[3]
M. MARCUS[3]
D. DERMATAS[2]
C. CHRISTODOULATOS[2]

[1]Department of Civil and Environmental Engineering
University of Connecticut Storrs CT 06269, U.S.A.
[2]Stevens Institute of Technology
Castle poiny on Hudson, Hoboken, 07030. NJ, USA
[3]Advanced Light Source, Lawrence Berkeley National Lab,
1 Cyclotron Rd., Berkeley, 94720, CA, U.S.A

ABSTRACT

The speciation of Cr(VI) in Cromite Ore Processing Residue was investigated by means of bulk XRD, and a combination of micro-XRF, - XAS and –XRD at the Advanced Light Source (ALS), Berkeley, CA, U.S.A.. Bulk XRD yielded one group of phases that contained explicitly Cr(VI) in their structure, Calcium Aluminum Chromium Oxide Hydrates, accounting for 60% of the total Cr(VI). Micro-analyses at ALS yielded complimentary information, confirming that hydrogarnets and hydrotalcites, two mineral groups that can host Cr(VI) in their structure by substitution, were indeed Cr(VI) sinks. Chromatite ($CaCrO_4$) was also identified by micro-XRD, which was not possible with bulk methods due to its low content. The acquisition of micro-XRF elemental maps enabled not only the identification of Cr(VI)-binding phases, but also the understanding of their location within the matrix. This information is invaluable when designing Cr(VI) treatment, to optimize release and availability for reduction.

1. INTRODUCTION

Chromite Ore Processing Residue (COPR) is generated as a by-product of the chromite ore processing to isolate and extract chromium. Chromite ore, which may be expressed by the chemical formula $(Mg, Fe)(Cr,Al,Fe)_2O_4$, is formed by means of a high-temperature (ca. 1200 ^{o}C) roasting process. Addition of lime during the roasting process leads to the formation of insoluble phases that are removed as solid waste, while Cr is recovered in the form of soluble chromate (CrO_4^{2-}) (Allied Signal, 1982). COPR has a residual chromium content, which may be up to 50,000 mg kg^{-1} total chromium, up to 50% of which may occur as Cr(VI). Hexavalent chromium is a known human carcinogen, rendering COPR a hazardous waste. To provide a basis for comparison, the Cr(VI) clean-up standard for residential use contaminated soil set by the New Jersey Department of Environmental Protection (NJDEP) is 20 mg kg^{-1}, which is by two orders of magnitude less than the COPR Cr(VI) content.

There are numerous chromite ore processing plants throughout the world. Three plants were located in Hudson County, New Jersey and deposited 2.75 million tons of COPR in the period 1905-1976. Investigations at 150 residential and commercial sites led to their characterization as hazardous and studies conducted by NJDEP showed that hexavalent chromium posed a viable threat to human health in N.J. (Lioy *et al.*, 1992). A lawsuit was enacted against the owner of a 34-acre site (denoted as SA7) on the Hackensack river in Jersey City, NJ, leading to the digging and hauling of 1.5 million tons of COPR. The site owner sought an alternative solution and initiated an extensive remedial investigation (Dermatas *et al.*, 2006a and 2006b).

Cr(VI) remediation is performed by reducing it to non-toxic trivalent chromium by means of chemical reductants, such as ferrous sulfate ($FeSO_4$) and calcium polysulfide (CaS_5). An essential prerequisite to successful treatment is the release of Cr(VI) from the solid matrix into solution, where it reacts with the added ions (ferrous iron or sulfide ions) and is reduced to Cr(III). Thus, the speciation of Cr(VI) in the solid is of fundamental importance for treatment design. Non-destructive techniques, such as X-ray Diffraction (XRD) and Scanning Electron Microscopy coupled with Energy Dispersive X-ray (SEM/EDX) can provide insight into Cr(VI) speciation, with some limitations. Chrysochoou and Dermatas (2007) employed quantitative XRD coupled with mass balances and found that approximately 50% of Cr(VI) in COPR was bound in a group of cementitious phases called Calcium Aluminum Chromium Oxide Hydrates (CACs). SEM/EDX analyses showed that there are also other cementitious phases with mixed chemical composition that contained Cr, however, no distinction between Cr(III) and Cr(VI) could be made (Chrysochoou 2006). Hillier *et al.* (2007) have reported hydrogarnet as an important sink for Cr(VI), but without specific spectroscopic data to support it.

This study presents the results of speciation analyses performed on COPR coupling XRD, SEM and micro-XAS analyses.

2. MATERIALS AND METHODS

A representative COPR sample obtained from SA7 was used for the analyses. The sample was a grey-black granular material. A standard thin section (30 µm thickness) of this sample was prepared using a diamond polish for microscopy and micro-XAS analyses.

The total Cr content was determined by acid digestion (U.S. Environmental Protection Agency method 3010) and Inductive Coupled Plasma/ Optical Emission Spectrometry (ICP/OES) (USEPA method 6010B). The Cr(VI) content was determined by alkaline digestion (USEPA method 3060A) and colorimetric analysis (USEPA method 7196).

The samples were air-dried for 24 h and mechanically pulverized to fit into a U.S. standard #400 sieve (37 µm). Step-scanned X-ray powder diffraction (XRPD) data were collected by the Rigaku DXR 3000 computer-automated diffractometer using Bragg-Brentano geometry. The diffractometry was conducted at 40 kV and 30 mA using a diffracted beam graphite-monochromator with a Cu radiation (λ=1.54Å). The data were collected in the range of two-theta values between 5° to 65° with a step size of 0.05^{o} and a count time of 5 seconds per step. The qualitative analysis of the XRPD patterns was performed using the Jade software (version 7.0). In order to assess the quantitative distribution of the identified crystalline phases the Whole Pattern Fitting function of Jade was used. We used the PDF-2 set of the International Center for Diffraction Data database, and the Inorganic Crystal Structure Database as reference databases for powder diffraction and crystal structure respectively.

Air-dried samples were mounted on carbon coating and analyzed by Scanning Electron Microscopy and Energy Dispersive X-ray (SEM/EDX) using a LEO 982 Field emission scanning electron microscope with an Oxford energy dispersive X-ray analyzer

Micro X-ray fluorescence (µXRF) elemental mapping, micro X-ray diffraction (µXRD), and micro X-ray absorption near edge structure (XANES) spectroscopy measurements described here were performed on Beamline 10.3.2 of the Advanced Light Source, Lawrence Berkeley National Lab, CA, USA. The hard X-rays beam spot size was adjustable from 5x5 µm^2 up to 16x7 µm^2. Micro-XRF mapping shows chemical associations, e.g., between trace and major elements. We then selected some spots of interest on which to perform XRD; which tells us what the dominant minerals are in the probed volume. Micro-XANES yields information about the redox state of Cr as well as the relative abundance between the two states (trivalent and hexavalent). This beamline is described in detail in Manceau *et al.* (2002). Micro diffraction was performed with a Bruker SMART 6000 CCD. The incident beam energy was set to 17 keV, which was high enough to perform XRD in transmission mode on the sample and provided access to reflections with d-spacings down to 1.24 A°. XRD Patterns were recorded for 10 min with a beam size of 16x7 µm^2. Patterns were calibrated using alumina powder and XRD profiles were extracted using the Fit2d software. Peak indexing and subsequent processing were performed with the Jade software, as with the bulk XRD patterns.

3. RESULTS AND DISCUSSION

The total Cr content of the soil was 21300 mg kg^{-1} and the Cr(VI) content was 4840 mg kg^{-1}, or 23% of the total Cr. This distribution is considered typical for grey black COPR samples from the SA7 site.

The mineralogy of the sample also represented the average mineralogy encountered in this type of material. Table 1 presents the quantitative mineralogy of the sample. Two CACs in different hydration states (12 and 14 water molecules) were detected in the sample, at ~2% wt. each. This amount corresponds to 2950 mg kg^{-1} or 60% of the total Cr(VI) in the sample. Furthermore, hydrotalcites (sjoegrenite and quintinite) are also layered-minerals with a potential to host chromate in their interlayer. Katoite (member of the hydrogarnet group) was also detected and is a potential Cr(VI) host, as previously noted. Finally, ettringite is theoretically a host for Cr(VI), although experimental studies have shown that it is dominated by sulfate (Chrysochoou and Dermatas, 2006).

It should also be noted that Cr(VI) could be present in phases that are not detectable by XRD, either due to detection limit (estimated at 1 wt.% for most COPR phases) or due to poor crystallinity. Sorption on iron surfaces is not a significant mechanism at pH 12.5 (Sposito, 1989).

Table 1. Quantitative Bulk XRD results for the COPR sample

	Chemical formula	**% wt.**
Brownmillerite	Ca_2FeAlO_5	25.9
Periclase	MgO	2.2
Brucite	$Mg(OH)_2$	3.9
Calcite	$CaCO_3$	6.7
Quartz	SiO_2	2.8
Katoite	$Ca_3Al_2(OH)_{12}$	13.3
Quintinite	$Al_2Mg_4(OH)_{12}(CO_3)(H_2O)_3$	2.6
Sjögrenite	$(Mg_6Fe_2(OH)_{16}(CO_3)(H_2O)_4$	3.6
Afwillite	$Ca_3Si_2O_4(OH)_6$	3.1
Ettringite	$Ca_6Al_2(OH)_{12}(SO_4)_3 \cdot 26H_2O$	1.3
CAC*	$Ca_4Al_2O_6(CrO_4) \cdot 14H_2O$	3.9
Amorphous		31.0

*CAC: Calcium Aluminum Chromium Oxide Hydrate

These preliminary results were then used as a basis to interpret the synchrotron based µXAS and µXRD data. Figure 1a shows an optical image of the COPR thin section, as observed through a camera that enables navigation on the sample during the analysis. The white square shows the area, where µXRF mapping was performed.
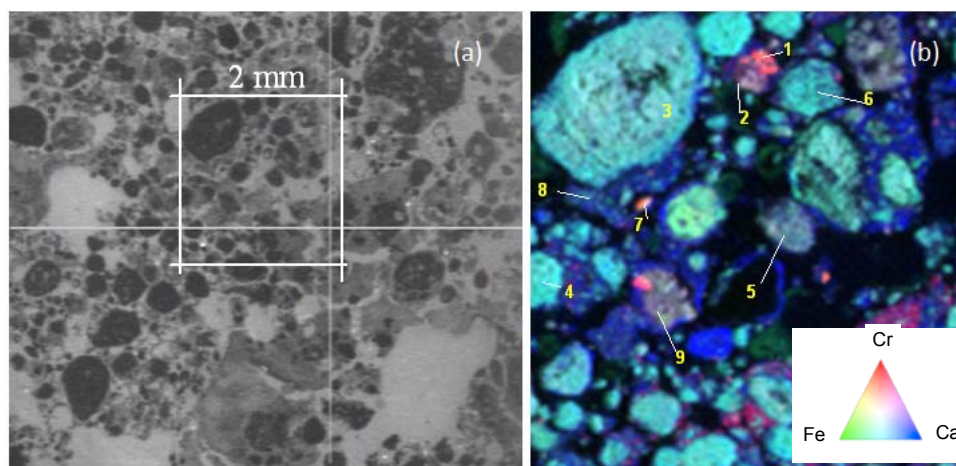

Figure 1. Optical image of COPR thin section (a) and XRF map of white square (Ca-blue, Fe-green, Cr-red)

COPR is a very heterogeneous matrix. The dark areas (or nodules) are variable in size and shape, and are not compact, but contain different particles within, as shown in higher magnification. They are generally surrounded by a dark grey cementing matrix, which also exhibits significant heterogeneity. The light grey areas represent void space. The heterogeneity may indicate that investigating COPR thin sections in a statistically relevant manner is a challenging task. However, the analysis of various COPR thin sections indicates that the optical images have similar features, with the combination of nodules and cementing matrix. Still, the analysis of this area is presented as a sample of the approach adapted and not as all-encompassing dataset for the material properties,

Figure 1b shows the tricolor XRF map of the square area. Along with Cr, the Ca and Fe distributions are also displayed since they represent the major COPR metals (20.5 wt.% and 10.9 wt.%, respectively). Al and Mg are also important metals, but those elements are not accessible at beamline 10.3.2 due to limits on the available energy range (S K up to Pb L_3). As expected, the map shows that Ca is ubiquitous and associated with Fe in the interior of nodules. Fe seems to be present predominantly in the nodules, with very little to none in the cementing matrix. It is believed that this is because Fe is predominantly associated with brownmillerite, the COPR parent mineral, which is found in the nodules. When brownmillerite hydrates, iron precipitates as amorphous iron hydroxide and is not incorporated in the hydration products that make up the cementing matrix [6].

Bright Cr spots were observed on several regions, along with some diffuse Cr-Ca rich areas (shown in purple on the map). It should be noted that the spot intensity may be misleading, because of the concentration of Cr in different minerals. For example, chromite ($FeCr_2O_4$) contains 46 wt.% Cr, while the CACs only 8%. Thus, chromite would appear as a bright red spot on the XRF map, while CACs or other Cr(VI) phases could be faint red or purple. Cr K-edge XANES was then performed on selected spots, marked as 1 through 9 in Figure 2.
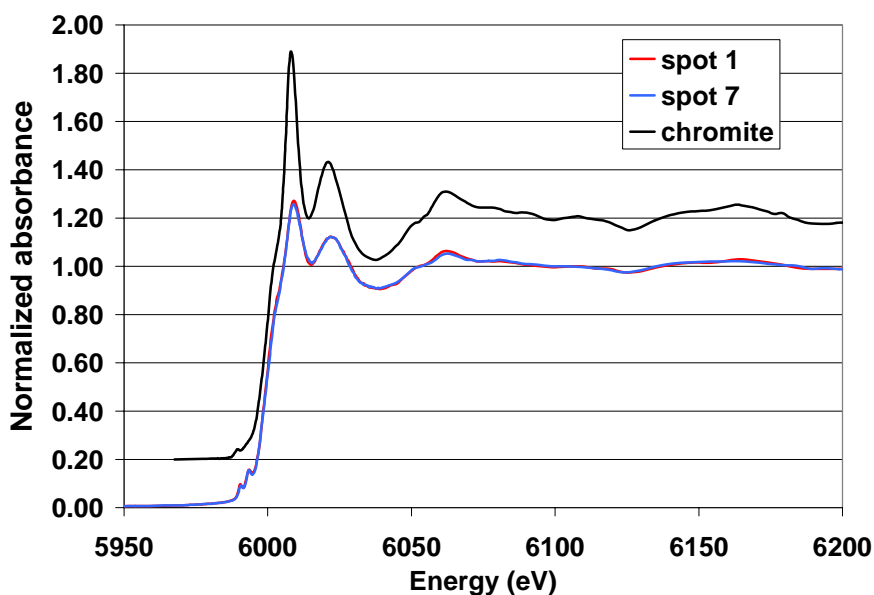

Figure 2. Normalized XAS spectra of spots 1 and 7 along with chromite ($FeCr_2O_4$). The spectrum of chromite was shifted vertically for clarity

Figure 2 compares the XAS spectrum of the bright red spots 1 and 7 with the spectrum of pure chromite. Spots 1 and 7 yielded identical spectra, with good agreement with the pure chromite spectrum. A small Cr(VI) peak was observed at 5993 eV, which could be due to the presence of another phase in the 7x16 μm^2 spot. Chromite was not identified in the bulk XRD pattern, because of the small residual amount (~1-2%) left in COPR, but it was observed in other COPR XRD patterns and in SEM (Chrysochoou, 2006). Small differences between the XANES spectra of spots 1 and 7 and to pure chromite can be attributed to the fact that chromite in COPR is not a pure phase but contains Mg, Al and trace Ti. Thus, the conclusion that bright red spots are probably associated with Cr(III) minerals and specifically chromite, was confirmed by this observation.
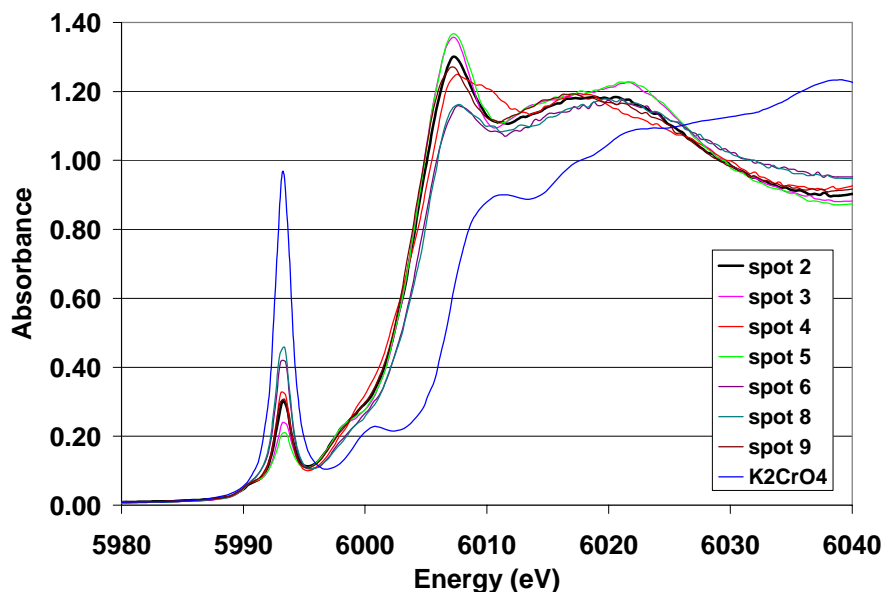
Figure 3. XAS spectra of the remaining spots compared to pure K_2CrO_4

Figure 3 shows the XAS spectra of the six remaining spots. A narrower energy region was chosen compared to figure 3 to facilitate the comparison between the seven spectra. All six spots exhibited the characteristic pre-edge feature at 5993 eV that signals the presence of Cr(VI). The post-edge spectrum of the spots was very different from that of potassium chromate, suggesting a different electronic configuration of the chromate anion in the structures that bind it. The post-edge spectra of the spots were, however, very similar, with the exception of spot 4 that exhibited a minor difference at 6010 eV. This finding suggests that Cr(VI) was bound in phases with similar structure in the analyzed spots. The peak height was variable, ranging from 20 to 50% the peak height of K_2CrO_4, which indicates that the amount of bound chromate varied, even though the electronic configuration was similar.

The XRD analyses of spots 4 through 9 showed that multiple minerals were present in most of the patterns, indicating that the spot size was too large to isolate individual Cr(VI)-bearing phases. Furthermore, a large background due to scattering of the substrate, the glass and the air rendered the positive identification of phases difficult. However, some preliminary conclusions were drawn from the analysis of the patterns. Figure 5 and 6 shows the patterns of spot 9 as characteristic examples.

CACs were not identified in any of the XRD patterns, even though they account for 60% of the total Cr(VI), according to bulk XRD. This confirms the previous observation, that a statistically significant analysis via microstructural methods requires the analysis of extensive areas and/or multiple samples. However, this was suitable for the purposes of the analyses because the objective was to identify other Cr(VI)-bearing phases, not the known CACs. No peaks were identifiable in spot 4, which had a slightly different XAS pattern than other phases. Thus, the phase was either amorphous to X-rays, or could not be identified due to the high background. Spot 5 contained brownmillerite, katoite and sjoegrenite. Both latter phases are potential Cr(VI) hosts, as previously noted. Spot 6 had a high Cr(VI) peak in the XANES spectrum and a pronounced katoite peak, along with some brownmillerite. This finding confirms the hypothesis that hydrogarnet acts as a Cr(VI) host in COPR. Spot 8, which had the highest Cr(VI) intensity in the XANES spectrum contained sjoegrenite and a peak at d-spacing 2.56 Å, which could not be identified. Spots 6 and 8 had almost identical XAS spectra, but different phase assemblages in XRD. This is a surprising finding that requires further investigation. Finally, spot 9 contained a pronounced peak of chromatite ($CaCrO_4$), along with some traces of other COPR phases (see figure 5). Chromatite is a mineral of relatively high solubility compared to other cement phases and is not predicted as a stable phase by geochemical modeling (Chrysochoou and Dermatas, 2005). It was also not identified in any of the bulk XRD patterns at SA7 (Chrysochoou, 2006), most probably because it was below the XRD detection limit.
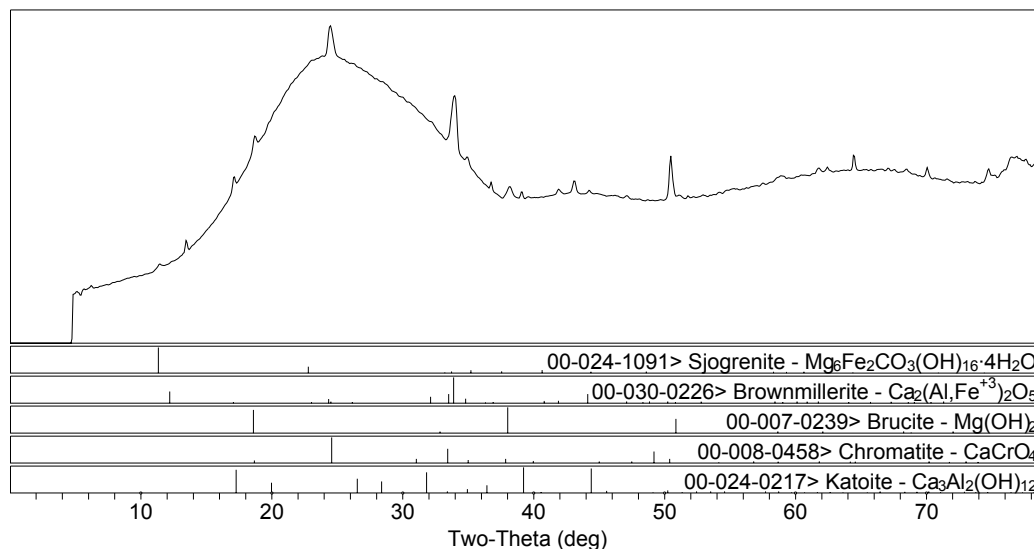
Figure 4. XRD pattern collected on spot 9

CONCLUSIONS

The speciation of Cr(VI) in Cromite Ore Processing Residue was investigated by means of bulk XRD, and a combination of micro-XRF, - XAS and –XRD. Bulk XRD yielded one group of phases that contained explicitly Cr(VI) in their structure, Calcium Aluminum Chromium Oxide Hydrates. Accounting for 60% of the total Cr(VI). Micro-XRF has shown the presence of several Cr hot spots, as well as weaker, more diffuse signals associated with Ca. Cr K edge XANES analysis on the hotspots showed that they were associated with the presence of residual chromite, containing little or no Cr(VI). The latter was observed in the more diffuse spots, and the spectra of several of the spots were similar, indicating similar electronic configurations around the chromate anion. The XRD results on the same spots yielded different phases, including katoite (hydrogarnet), hydrotalcite and chromatite.

Overall, the combination of these analysis enabled the positive identification of Cr(VI)-bearing phases that were only speculated sinks thus far, as well as the identification of phases below the bulk XRD detection limit. More work is required in larger areas and more samples to obtain better statistics. The beamline enables the acquisition of Cr(VI) maps over entire sample areas, significantly improving the understanding of Cr(VI) presence within the matrix and providing a better platform to conduct micro-XANES and micro-XRD analyses. This type of information cannot be obtained by any other experimental method and constitutes valuable information for Cr(VI) release and treatment.

ACKNOWLEDGMENTS

REFERENCES

Allied Signal (1982), 'Process Descriptions Baltimore Plants'

Chrysochoou M., (2006), Investigation of environmental and geotechnical implications associated with deposition of Chromite Ore Processing Residue (COPR). Ph.D. dissertation, Stevens Institute of Technology, Hoboken, NJ, U.S.A.

Chrysochoou M. and Dermatas D., (2005), Comparison of geochemical modeling in Chromite Ore Processing Residue using MINTEQ and EQ3/6 software, Proceedings 9th Conference on Environmental Science and Technology, Rhodos, Greece.

Chrysochoou M. and Dermatas D., (2006), Evaluation of Ettringite and Hydrocalumite Formation for Heavy Metal Immobilization: Literature Review and Experimental Study, *Journal of Hazardous Materials*, **136**(1), 20-33.

Chrysochoou M. and Dermatas D., (2007), Application of the Rietveld method to assess Cr(VI) speciation in Chromite Ore Processing Residue, *Journal of Hazardous Materials*, **141**(2), 370-377.

Dermatas D., Bonaparte R., Chrysochoou M. and Moon D.H., (2006a), Chromite Ore Processing Residue: Hazardous Contaminated Soil or Solid Waste?, *Journal of ASTM International*, **3**(7), (doi: 10.1520/JAI13313).

Dermatas D., Chrysochoou M., Moon D.H., Grubb D.G, Wazne M. and Christodoulatos C., (2006b), Ettringite-Induced Heave in Chromite Ore Processing Residue (COPR) upon Ferrous Sulfate Treatment, *Environmental Science and Technology,* **40**(18), 5786-5792.

Hillier S., Lumsdon D.G., Brydson R., Paterson E., (2007), Hydrogarnet: a host phase for Cr(VI) in Chromite Ore Processing Residue (COPR) and other high pH wastes, *Environmental Science and Technology*, **41**, 1921-1927.

Lioy P.J., Freeman N.C.G., Wainman T., Stern A.H., Boesch R., Howell T. and Shupack S.I., (1992), Microenvironmental analysis of residential exposure to chromium-laden wastes in and around New Jersey homes, *Risk Analysis,* **12**, 287-299.

Manceau A., Marcus M.A. and Tamura N., (2002a), Quantitative speciation of heavy metals in soils and sediments by synchrotron X-ray techniques. In Applications of Synchrotron Radiation in Low-Temperature Geochemistry and Environmental Science, **49**, 341–428.

Sposito G., (1989),. The chemistry of soils, Oxford University Press, New York.